THE AMERICAN SOCIETY OF MECHANICAL ENGINEERS
345 E. 47 St., New York, N.Y. 10017

91-GT-83

The Role of Tip Clearance in High-Speed Fan Stall

J. J. ADAMCZYK
NASA Lewis Research Center
Cleveland, OH 44135

M. L. CELESTINA
Sverdrup Technology, Inc.
Lewis Research Center Group
Cleveland, OH 44135

E. M. GREITZER
Massachusetts Institute of Technology
Cambridge, MA 02139

ABSTRACT

A numerical experiment has been carried out to define the near stall casing endwall flow field of a high-speed fan rotor. The experiment used a simulation code incorporating a simple clearance model, whose calibration is presented. The results of the simulation show that the interaction of the tip leakage vortex and the in-passage shock plays a major role in determining the fan flow range. More specifically, the computations imply that it is the area increase of this vortex as it passes through the in-passage shock, which is the source of the blockage associated with stall. In addition, for fans of this type, it is the clearance over the forward portion of the fan blade which controls the flow processes leading to stall.

INTRODUCTION

A characteristic feature of high-speed, high pressure ratio axial compressor rotors is the limited range of stable operation at design speed, often as little as ten percent of the design flow. To use these high performance rotors to best advantage in an aeropropulsion system, it is thus desirable to develop methods for increasing this flow range. Understanding the underlying phenomena that control fan stall and stability is an important part of this problem.

In the last decade, there has been considerable progress in understanding and modeling of stall and surge of axial flow compression systems. See, for example, the work of Moore (1984), Moore and Greitzer, Greitzer and Moore (1986). Existing stability models, however, take as input the pressure characteristic map of the compressor. None of the models advanced in the open literature describe the detailed flow phenomena occurring within the blade row passage which gives the characteristic its shape at stall. This is an important piece of the problem because it determines not only the base flow from which an instability evolves but also the nature of the instability.

The objective of the present work is to identify, using numerical simulation, the base flow from which an instability can develop in the tip region of a high-speed fan rotor, for it is well known that stall of modern fan rotors often originate in this region. Put another way, what is aimed at here is an answer to the fluid dynamic question of what are the dominant phenomena that are involved in the fan stall process? A principal component of the answer to this will be shown to be the strong interaction between the tip leakage vortex an the in-passage shock system.

BACKGROUND: TIP CLEARANCE FLOWS AND EFFECTS ON COMPRESSOR STABILITY

Many researchers have documented the importance of tip clearance on the stability boundary of axial flow compressors. Smith (1970) showed that increasing the clearance between the tips of rotors and the casing of a low speed compressor caused the point of stall inception to move to a higher flow rate. Similar results were reported by Moore (1982), Freeman (1985) and Wisler (1985) for high-speed machinery. The role of tip clearance is also brought out in the correlation of Koch (1981), and Schweitzer and Garberoglio (1983).

An early attempt at examining the in-passage shock system at the tip of a transonic rotor was made by Miller and Bailey (1971), who measured the shroud pressure distribution over the tip of several rotors. We show these distributions to illustrate the general features of the problem that is addressed. Figure 1, taken from their report, shows two plots, at choke and near stall condition. The location of the in-passage shocks, and the leakage vortex, inferred from the contours, have been added by the authors. At choke flow the contours suggest that the shock system consists of a series of oblique waves which propagate across the blade channel without noticeable distortion. There is no clear evidence of a leakage vortex. At the near stall point the contour plot shows the

Presented at the International Gas Turbine and Aeroengine Congress and Exposition
Orlando, FL June 3-6, 1991
This paper has been accepted for publication in the Transactions of the ASME
Discussion of it will be accepted at ASME Headquarters until September 30, 1991

shock system is a single nearly normal wave standing in front of the entrance to the blade channel. The low pressure trough which forms near the leading edge of the suction surface is the signature of the leakage vortex which forms as a result of the encounter between the clearance flow and the flow entering the blade channel from upstream. Where the vortex intersects the in-passage shock, there is a local distortion of the contours which implies a strong interaction between the shock and the vortex.

Another perspective on the rotor endwall flow field is provided by the laser holograms of Nicholas and Freeman (1982). Figure 2, a photographic reproduction of one of their holographic images, shows the shape of the in-passage shock as well as the leakage vortex. Their report, like those noted previously, points to the importance of clearance in determining the stall limit.

The studies cited show that tip clearance effects play a major role in setting the stall limit, but they do not draw any clear, causal connections between endwall flow structure and instability onset. A main reason for this is the inherent complexity of the former. For example, features of the endwall region that can be significant are: clearance flow, associated leakage vortex and its behavior in an adverse pressure gradient, incoming casing boundary layer, and, for high-speed machines, passage shock system. The central point is that the behavior of interest is the resultant of an interaction among the various items and it is only in recent years that the capability to examine the interaction via numerical simulation has been developed.

In this context, a useful resolution of at least part of the question was provided by Crook (1989) who executed a series of numerical simulations of the endwall flow in a low speed machine. Crook examined the flow with and without casing treatment, although we only discuss the smooth wall situation here. In the simulation, the flow from the clearance was seen to evolve into a vortex which grew in cross section as it encountered the adverse pressure gradient in the passage. The region of high loss at the rear of the passage was essentially the core of the vortex. The result, taken with the data reported by Miller and Bailey (1971) and Nicholas and Freeman (1982) suggests that similar phenomena arise as a result of the interaction between the leakage vortex and the in-passage shock system. Later in this paper, we will present the results of several simulations which suggest that, under certain operating conditions, the low energy fluid generated by this interaction spills forward raising the blockage in the forward portion of the blade passage causing the flow system to become unstable.

Flow spillage forward of the blade passage has been previously suggested as triggering the onset of stall (McDougall et al., 1990). The connection between spillage and stall inferred from the computations reported herein, however, is only that they occur as parts of the same process. Whether the spillage is a cause or a result of the stall onset is an aspect of the stall transient that is beyond the scope of this paper; the goal here is rather to elucidate those features of the (pre-stall) flow which can be directly linked to the breakdown of steady state conditions.

The remaining portion of this paper is divided into three parts. The first presents an overview of the numerical solution procedure and a description of the clearance flow model. It also contains comparisons between simulations and measurements, which serve to calibrate the simulation code. The second part focuses on the casing end-wall flow at a near stall condition. The last part presents a series of simulations designed to substantiate the inferences drawn from the second section.

CALIBRATION OF THE NUMERICAL SIMULATION CODE

The code used in the present study is based on a finite volume discretization of the Reynolds-Averaged form of the Navier-Stokes equations. The temporal integration procedure is a four stage Runge-Kutta scheme. The details of the simulation code, including a description of the artificial damping operator, the turbulence model, and the boundary conditions can be found in Adamczyk et al. (1989). The flow in the clearance gap was simulated using a model suggested by Kirtley et al. (1990). The flow is taken to be transported tangentially through the gap with no loss in mass, momentum or energy. The effect of the vena contracta is accounted for by choosing the clearance to be smaller than the actual clearance. The model leads to the formation of a wall jet which interacts with the oncoming flow in the passage.

At the solid boundaries, the simulation code used wall functions to estimate the wall shear stress when the value of y^+ at the center of the first mesh cell away from the wall boundary exceeded thirty. (y^+ is the distance normal to a solid surface nondimensionalized by the square root of the ratio of the wall shear stress to the fluid density at the surface and the kinematic viscosity.) For values of y^+ less than thirty, the wall shear stress was evaluated from the gradient of the velocity vector at the wall. The eddy viscosity at the cell adjacent to the wall was estimated consistent with the procedure used to estimate the wall shear stress.

The simulations were of the NASA Lewis Rotor 67, whose measured performance is reported by Strazisar et al. (1989). The rotor is a 1.56 aspect ratio transonic design with a tip relative Mach number of 1.38. The measured efficiency is over ninety percent at design speed.

The grid used in the simulations had thirty-one cells in the radial and circumferential directions. One hundred and five cells were placed between the inlet and exit boundaries, of which forty-one were along the blade chord line. The clearance gap was spanned by two cells in the radial direction. The grid in the clearance gap region above the rotor tip is constructed by simply extending the grid below the tip to the shroud while maintaining the tangential distance across the blade passage fixed to its value at the rotor tip. The number of grid points spanning the gap in the radial direction would be too few if one were interested in resolving the details of the flow entering and exiting the gap (see Crook, 1989 for a description of these regions). In the present study however, we are interested mainly in clearance flow as it interacts with the primary stream out in the blade passage. Several studies have shown that reasonable estimates of this interaction can

be obtained without a detailed description of the flow exiting the gap if one has a good estimate of the gap mass flow. This can be accomplished in a numerical simulation with as few as one grid cell spanning the radial direction if one accounts for the blockage introduced by the vena contracta.

To show the ability of the simulation code to capture the correct trends, computed and measured adiabatic efficiency and pressure ratio at design speed are presented in Figure 3. The abscissa for both curves is the ratio of the mass flow rate to the mass flow rate at choke. The exit total pressure is a mass averaged value normalized by the inlet mass-averaged value. Agreement between computation and experiment is good. Further, the shape of the predicted efficiency curve is consistent with the reported curve, the predicted flow rate at peak efficiency being nearly equal to the measured value. The only apparent discrepancies are a slight over-estimate of the pressure rise near max flow and the underprediction of the efficiency.

The predicted pressure level and the flow rate at stall also agree reasonably well with the measured values. Note that in the present paper, the stall point in the simulation is defined as the flow rate corresponding to the maximum pressure ratio for which the numerical simulation would converge (i.e., stall onset is taken as the flow rate below which the simulation will not converge). All attempts to find a steady solution for mass flows less then this value produced a transient response where the mass flow at the inlet steadily decreases as the solution was marched forward in iteration cycle, terminating in a reversed flow region at the inlet and divergence.

Figure 4 shows the radial distribution of the computed and measured mass-averaged total pressure and total temperature profiles downstream of the rotor for peak efficiency and near stall operation. Again agreement between the simulation and the measured values is good, the only disagreement being a slight over-prediction of the pressure at peak efficiency. However, and this is the main point of Figures 3 and 4 (as well as the more detailed comparisons in Figures 5 and 6), the parametric dependence is well captured so that there is confidence in the use of the code for numerical experimentation.

A third assessment of the simulation is given in Figures 5 and 6 which show intra-blade Mach number distributions. The experimental results were estimated from LDV measurements of the velocity field. The plots are for ninety and seventy percent of span as measured from the hub. The contours from the simulation and those estimated from the measured velocity field are in good agreement, as is the location of the in-passage shock implied by the contours. The latter is important because the shock plays a key role in forcing the clearance flow through the gap.

As stated, the results confirm the suitability of the simulation code for a qualitative study of the shroud end-wall flow. They indicate that the code is capable of predicting loading level, and shock position. Discrepancies between prediction and measurement are judged to be sufficiently minor so as not to affect the conclusions concerning physical mechanisms that are drawn from the simulations which follow.

PREDICTION OF CLEARANCE EFFECTS ON ROTOR PERFORMANCE AND ENDWALL FLOW STRUCTURE

Overall Behavior. A series of simulations of Rotor 67 were executed at clearance to tip chord ratios of zero, 0.25%, 0.75% and 1.25%. These span the range found in modern high-speed fans. For each clearance, pressure and efficiency maps were computed along a line of constant corrected speed. The speed lines include the point of stall onset, which (as stated) is defined to be the point of operation at which any increase in the exit static pressure results in a steady decrease in the mass flow at the inlet as the solution iteration cycle count is advanced. (One might interpret this behavior as an indication that the pressure characteristic has reached its maximum so the slope of the characteristic is either zero or possibly discontinuous.) The endwall flow field will be analyzed near this point to define the flow field from which the instability evolves.

The computed pressure rise and efficiency are shown in Figure 7 for the four clearances. Increasing the clearance from zero results in a decrease in rotor pressure rise capability and a reduction in operating range. On the other hand, the efficiency has a maximum at a non-zero clearance. Although no direct comparison is made, these trends are consistent with those reported in the experimental studies of Freeman (1985) and Wennerstrom (1984).

Endwall Flow Field. In this section we will examine in some detail the results from simulations done at three different clearances. The first is the nominal clearance of 0.25 percent of tip chord, which might be a tight clearance in a modern fan. This will show the effects that are to be expected from vortex-shock interaction in such a situation. A larger clearance, 1.25 percent of tip chord, will then be considered. Although the behavior is qualitatively the same, because of the larger clearance (and hence larger leakage vortex), this set of computations illustrates in a more evident manner, the influence of the shock vortex interaction. Finally we consider the situation with zero clearance, which will be seen to be qualitatively different than either of the first two cases, because of the absence of the leakage vortex.

Nominal Clearance (0.25 Percent Tip Chord) Flow Field. Figure 8 shows the relative total pressure and static pressure distributions on a surface of revolution at 99.85 percent of span as a function of nondimensional axial tip chord and pitch. The clearance to tip chord ratio is 0.25 percent, and the operating conditions are peak efficiency, and near stall. The nondimensional pitch and axial tip chord each vary from zero to one with zero pitch corresponding to the pressure surface and zero axial chord corresponding to the rotor inlet plane. The line plots in this figure as well as those in similar figures which follow are drawn at 3, 5, 10, 15, 20, 25, 40, 60, 75, 85, 90, 95, and 97 percent of pitch.

The structure of the in-passage shock system at the rotor tip can be seen from the pressure plots. At peak efficiency the shock structure is a lamda pattern with both legs originating from the pressure surface, while near stall the pattern is that of a strong oblique wave which stands-off of the leading edge.

The leakage vortex can be tracked in the static pressure plots by the low pressure depression which forms near the leading edge of the suction surface, but it is more evident in the relative total pressure plots. In the latter its signature appears as a low pressure trough originating near the leading edge of the suction surface. As the rotor is throttled towards stall the relative total pressure in the core of the vortex decreases and the trajectory of the vortex across the blade passage becomes more tangential.

Slightly upstream of the impingement of the in-passage shock on the suction surface (i.e., near 0.70 axial tip chord at peak efficiency and 0.40 axial tip chord for the near stall point), there is a second region of low relative total pressure created by the interaction of the shock with the suction surface boundary layer and the fluid particles which have come through the gap from the adjoining blade passage. At the near stall point this low total pressure fluid is transported upstream by the fluid exiting the gap and entrained in the leakage vortex near 0.40 pitch and 0.25 axial tip chord. The total pressure in the core of the vortex is decreased by this process. This transport mechanism will be made evident by means of plots which show the path of fluid particles in the end-wall region. Upon encountering the shock the size of the vortex cross section is increased causing the low relative total pressure within the core to be spread laterally across the blade passage.

Figure 9 shows the flow structures which control the flow field at the tip of a rotor at the near stall operating condition. The upper portion of the figure shows an illustration which identifies these structures. The two key structures are the leakage vortex and the leakage flow from which it was formed and the in-passage shock. The blade geometry is also shown to give a perspective of the relationship between these structures and the geometry. The lower portion of the figure contains three plots in which the view is from the shroud looking in towards the hub. These plots quantify the structures identified in the illustration. The plot on the lower left shows, in the relative frame of reference, the paths of the fluid particles released upstream of the rotor inlet plane between the rotor tip and the shroud (99.85% of span) and restricted to an axisymmetric surface of revolution at 99.85 percent of span. This surface is between the shroud and the rotor tip. The middle plot shows the paths, in the relative frame of reference, of fluid particles released between the rotor tip and the shroud (99.85% of span) above the suction surface. The plot on the right shows contour levels of the axial velocity as viewed in the relative frame of reference on an axisymmetric surface of revolution at 99.85 percent of span. The location of the in-passage shock at the tip is shown in the plot on the bottom right, while the trace of the leakage vortex is noted by the line O-P on the lower middle plot.

The plot on the lower right shows that, near the shroud, the majority of the fluid particles approaching the rotor do not directly enter the blade passage. They appear to be blocked from doing so by a flow obstruction.

The formation of the leakage vortex is illustrated in the lower middle plot. These particles were released above the suction surface in the clearance region. These traces outline the leakage vortex (line O-P). A curve drawn through the furthermost upstream position of the paths of the particles released between the leading edge and mid-chord corresponds very nearly to the fluid particle path in the lower left plot originating from the suction surface leading edge. This result suggests the leakage vortex is acting as a flow obstruction which causes the flow entering the blade passage to pass around it rather than through it.

Contour levels of the axial velocity normalized by the wheel speed on a surface of revolution at 99.85 percent of span are shown in the lower right plot. The dashed contour is zero axial velocity. All the contours within the zero contour have a negative value, while those outside the zero contour have positive values. In the negative contour region, the fluid particles, in the relative frame of reference, travel upstream as they move across the passage. This motion, which can also be seen in the lower middle plot, is responsible for transporting the region of low relative total pressure originating near mid-chord in Figure 8 towards the leading edge vortex.

Figure 10 shows the relative total pressure distribution at near stall on cross sectional planes A-A and B-B as shown in Figure 9. These planes are nearly orthogonal to the vortex axis so the representation of the cross section dimension of the vortex structure is to scale. The abscissa in the plots is physical distance measured from the left edge of the sectional cut while the ordinate is the radius. The location of the suction surface relative to the sectional plane A-A is 1 percent of span and is noted on the figure. The location of the pressure surface relative to the sectional plane B-B is 0.4 percent of span and is also noted in the figure. All dimensions on this figure are nondimensionalized with respect to the span of the rotor at the leading edge. A-A is upstream of the in-passage shock and the cut at B-B is downstream of the shock as drawn in Figure 9. (The upper edge of the contour plots is not straight because the intersection of the shroud and the plane is not a line of constant radius. The shape of the lower edge is the result of the graphics routines used in the generation of these plots which draws the lower edge parallel to the upper edge.)

In both plots the contour level 2.3 represents the relative total pressure of the primary stream. By comparing contour level 2.1 in both plots one can see the growth of the vortex as it passes through the shock. (For reference, in these units the relative inlet dynamic pressure is roughly unity.) In agreement with Crook's (1989) observations, the region of low relative total pressure within the core of the vortex causes large growth of the vortex when it encounters a pressure rise. Most of the pressure rise in the present case is produced by the shock, while Crook (1989) based his observations on analyzing low speed machinery. The interaction he observed between the leakage vortex and the blade passage pressure field, however, also takes place in high-speed machinery, with the shock the generator of the adverse pressure gradient. It will be shown that suppression of this interaction can lead to an increase in the stable operating range of a rotor.

As the flow is reduced, the leakage vortex inclines more towards the tangential direction and the shock moves forward. As a result, the large blockage generated by the interaction of the vortex and the shock also moves forward. This produces

a region of low relative total pressure along the shroud near the pressure surface which spills forward initiating numerical stall. The spillage of low energy flow drives the bow shock at the leading edge of the tip blade section forward altering the upstream wave pattern, reducing the mass flow rate, and increasing the blade incidence. This increased incidence raises the blade loading, which, in turn, increases the leakage flow, driving the bow shock further forward. This series of events leads to a steady reduction of the mass flow as the simulation iteration cycle count is advanced and results in the simulation undergoing a rapid divergence when the region of low relative total pressure reaches the inlet plane of the computational domain. The mass flow rate just prior to the onset of this rapid divergence has dropped far below a level which is reasonable to expect stable operation of a high-speed machine. We, therefore, feel that there is physical significance to this point of instability. Furthermore, this point of operation coincides with the peak in the predicted pressure characteristic curve and, because of this, we suggest that the flow field at mass flows just above the predicted peak in the pressure characteristic cure may form the base flow from which rotating stall develops in an isolated fan rotor.

Increased Tip Clearance (1.25 Percent Tip Chord) Flow Field. The behavior just illustrated can be seen more clearly if we examine a rotor with larger tip clearance. This is done in Figures 11 to 13 which are derived from computations carried out with a tip clearance of 1.25 percent of tip chord. Figure 11 presents plots of the relative total pressure and the static pressure on a surface of revolution just inboard of the tip (99 percent of span). Both peak pressure and near stall conditions are shown. The format is the same as that in Figure 8, with zero values of pitch and axial chord corresponding to pressure side and leading edge plane, respectively.

If we compare the pressure distribution at near stall to that with the smaller tip clearance (Figure 8) we find the shock structure is qualitatively similar. There is, however, a lower pressure rise through the shock, and thus a reduction in pressure difference across the blade over the outer ten per cent of blade span.

The leakage vortex is indicated by the trough in relative total pressure observed originating from the suction surface slightly aft of the leading edge. Its trajectory is shown by the dashed line. Further aft along the suction surface there is another region of low relative total pressure (as with the .25 percent clearance) due to the shock interacting with the suction surface boundary layer and the flow which has come through the gap from the adjoining blade passage. At near stall the minimum relative total pressure, along the suction surface, is lower than that for .25 per cent clearance. At peak efficiency the low total pressure is transported tangentially into the blade passage by the clearance flow while at the near stall point the transport is not only tangentially but towards the rotor inlet plane. The transport process at the near stall condition will be illustrated below by means of a series of plots of fluid particle paths in Figure 12.

The upper portion of Figure 12 shows an illustration of the formation of the leakage vortex and its encounter with the in-passage shock at the near stall operating condition. The purpose of this illustration, as it was in Figure 9, is to aid the interpretation of the plots which appear in the lower portion of the figure. The view for Figures 12B, 12C, and 12D is from the shroud looking in toward the hub. The format for these figures is identical to that for Figures 9B, 9C, and 9D. Figure 9B shows the streamlines of the relative flow field on an axisymmetric surface of revolution located at 99 percent of span as defined by particle paths originating upstream of the rotor. This surface lies between the shroud and the rotor tip. The streamline originating from the leading edge divides the upstream flow from that which came through the clearance. This line is an indication of the forward edge of the leakage flow across the passage and its geometry near stall is similar to the corresponding streamline in Figure 9B. Figure 12C shows the paths of fluid particles released in the clearance region over the suction surface. The line O-P shows the trajectory of the vortex across the passage. The shock front at the shroud is shown in Figure 12B. The formation of the leakage vortex from the clearance flow is evident. Figure 12D is a contour plot of the axial velocity normalized with respect to the tip wheel speed on an axisymmetric surface of revolution at 99 percent of span. The dashed contour corresponds to zero axial velocity. The contours within the region bounded by the zero contour are negative while those that are outside are positive. In comparing Figure 12D with Figure 9D, it is clear that the larger clearance has resulted in a larger region of negative axial velocity. In fact, this region extends across the entire passage in Figure 12D while in Figure 9D it ends before it reaches the pressure surface. Within the region of negative axial velocity in Figure 12D the low relative total pressure found between twenty and fifty percent of axial chord in Figure 11 is transported towards the vortex and becomes entrained in the vortex prior to the in-passage shock. This is also evident in Figure 12C. As the flow is further reduced towards stall, the low energy flow associated with the clearance flow spills forward of the rotor inlet plane.

Figure 13 illustrates the vortex cross section at the near stall point using contour plots of the relative total pressure on sectional planes A-A and B-B. The planes are located on either side of the shock and are nearly orthogonal to the vortex trajectory. The format for the plots is identical to that for Figure 10. The location of sectional plane A-A relative to the suction surface is 0.18 percent of span, while the sectional plane at B-B is located at 0.21 percent of span relative to the pressure surface. These locations are noted in the figure. The contour plots in Figure 10 and 13 for section A-A shows that the larger clearance produces a larger vortex as is expected. (The vortex size should roughly scale on clearance (Chen et al., 1990)). The vortex cross section increases markedly in size upon passing through the shock, as can be seen by comparing contour level 2.1 on plane A-A in Figure 13 with the corresponding contour on plane B-B. This vortex growth is responsible for the sharp increase in endwall blockage as stall is approached. At numerical stall, this blockage increase forces the bow shock at the tip section forward causing a steady reduction in mass flow through the rotor as the simulation iteration cycle is advanced.

Zero Clearance Flow Field. It is instructive to compare the flow fields in the two above cases with that for zero tip clearance, where the structure is qualitatively different. Figure 14 shows the relative total pressure and the pressure distribution near the casing for zero clearance as a function of nondimensional pitch and axial tip chord at peak efficiency and near stall throttle setting. The scale is identical to Figure 8 and the mass flow rates for corresponding plots are nearly the same.

The shock structure for the near stall operating point is close to that in Figure 8. There is, however, a difference between the relative total pressure (in Figures 8 and 14) forward of .30 axial tip chord. The comparison illustrates the loss in relative total pressure that occurs as a result of the formation of the leakage vortex and the influence this loss generation mechanism has on the blockage in the forward portion of the blade passage. It is apparent at peak efficiency and especially so for the near stall operating point. However, even at peak efficiency, the clearance flow and the blockage it generates appears to have an impact on the shock structure. The relative total pressure plot in Figure 14 also shows a region of low pressure developing along the suction surface (pitch ratio of unity) near 0.50 axial tip chord. The low pressure results from the interaction of the in-passage shock with the suction surface boundary layer and grows in size as the rotor is throttled towards stall.

Figure 15 shows the paths of fluid particles released at the inlet plane to the rotor and restricted to an axisymmetric surface of revolution at 99 percent of span. The intent is to portray the streamlines near the shroud. Note the differences with Figures 9 and 12. Here, (Figure 12) there is little deflection of the streamlines because there is no leakage vortex. The blockage generated by the vortex deflects the incoming stream in the tangential direction.

Relation Between Low Energy Flow In Vortex and Stall Onset. The simulations discussed in the previous section showed a strong correlation between the onset of stall and the forward movement of low energy fluid which is connected with the clearance vortex. To examine this further, two sets of simulations were executed in which the growth of the blockage in the end-wall region was controlled by reducing the clearance to zero over the forward portion of the rotor only. For the first set, the clearance to tip chord ratio was zero to mid-chord, and 1.25 percent from there to the trailing edge. For the second set of results, the clearance ratio was zero to twenty nine percent of chord, and 1.25 percent from there to the trailing edge. These configurations yielded varying degrees of interaction between the clearance flow and the in-passage shock system.

The flow range associated with each of the partial clearance configurations as well as that of all the previously examined configurations is shown in Figure 16. The most significant result contained in this figure is the flow range that is obtained with the partial clearance. The two partial clearances are shown as the half solid symbols. The large change due to sealing the front part of the blade is evident. Specifically, the partial clearance with fifty per cent of the blade sealed could be throttled to a lower flow than the .25 percent configuration. Even sealing the blade over the front twenty nine per cent of blade yields a flow range near that of the .25 percent configuration.

The reason for this improvement can be seen in Figure 17, which presents near stall relative total pressure plots on an axisymmetric surface at ninety-nine percent of span. Four different configurations are shown, the nominal clearance (.25%) the large clearance (1.25%), zero clearance, and the fifty percent partial clearance. The first two of these can be seen to be at least qualitatively similar to each other, as are the latter two, but there is a substantial difference between the two pairs. With the partial clearance (as with the zero clearance), there is no leakage vortex in the front part of the blade passage. We associate the absence of the leakage vortex in the front part of the passage with the shift in the stall onset point.

An alternative presentation of the tip region flow field for the partial clearance configuration is given in Figure 18, which shows relative total pressure and static pressure at the near stall point on an axisymmetric surface of revolution at ninety-nine percent of span. The format of this figure is identical to that introduced in Figures 8 and 11, and the plots themselves are similar in appearance to those for zero clearance presented previously in Figure 15. The region of low relative total pressure found along the suction surface with zero clearance is also found in the present configuration although the loss in relative total pressure is less then that for zero clearance because of the high energy fluid which has come through the gap at the rear portion of the blade.

With the partial clearance, the interaction of the clearance flow with the primary passage flow is confined to the region aft of the shock. The end-wall flow in the middle of the passage approaching the shock has high relative total pressure. Suppression of the interaction of the shock with the low relative total pressure fluid associated with the leakage vortex has lead to a reduction in end-wall loss and blockage in the forward portion of the blade passage, producing the increases in stability shown in Figure 16. These results substantiate the important role played by the tip vortex in initiating the onset of stall and show the sensitivity of the stall point to the clearance over the forward portion of the fan blade.

SUMMARY AND CONCLUSIONS

1) A numerical experiment was performed to document the structure of the near stall end-wall flow field in a high speed rotor. Tip clearance was varied from zero over a range representative of modern fans so the influence on the structure of the end-wall flow could be seen.

2) Analysis of the runs with clearance showed a build-up of low energy fluid along the casing due to the interaction of the clearance vortex and the in-passage shock. This region of low energy fluid grew and moved forward as the flow rate was decreased. At a critical value of the flow rate, the region of low energy fluid rapidly moved forward with corresponding increases in loss and blockage. The numerical simulation would stall at this point, being unable to converge to a solution.

3) The zero clearance computation showed an increased flow range compared to results with clearance, due to the absence of vortex-shock interaction.

4) Simulations were also carried out with zero clearance over the forward portion of the fan rotor but a large clearance over the aft part. The rotor exhibited a large stable operating range, again because of the reduction in vortex-shock interaction. These results show the strong dependence of the flow range on the clearance over the forward portion of the blade.

5) From the present study it appears that injection of high energy fluid in the forward part of the casing end-wall region to reduce or eliminate the growth of low regions of relative total pressure would have a beneficial effect on flow range. As noted by Crook (1989), axial groove casing treatment appears to provide such an injection mechanism.

6) It would be worthwhile to examine the end-wall flow structure in a multi-stage axial flow compressor to see whether the findings of the present study are relevant to multi-stage machinery.

ACKNOWLEDGMENTS

The authors wish to acknowledge the extent to which this work was stimulated by the initial numerical experiments and their analysis by Mr. A. Crook of Allison Gas Turbine Division. Mr. Crook's work provided much useful insight into the importance of the clearance vortex for the end-wall flow. We are also grateful to Professor N. A. Cumpsty of Cambridge University for helpful comments as well as to Mr. D. J. Nicholas and Mr. C. Freeman of Rolls-Royce Derby for providing reproductions of their holographic photographs and a copy of their very informative paper. The comments of Dr. I. J. Day concerning his measurements are also appreciated. We would further like to thank Dr. K. Dugas for her invaluable help with the manuscript. Support for E. M. Greitzer in this work is from NASA Lewis Research Center under Grant NSG-3208, Mr. F. A. Newman Contract Monitor. This support is gratefully acknowledged.

REFERENCES

Adamczyk, J.J., Celestina, M.L., Beach, T.A., and Barnett, M., 1989, "Simulation of Three-Dimensional Viscous Flow Within a Multi-Stage Turbine," ASME Journal of Turbomachinery, Vol 112, No 3, pp 370-376.

Chen, G.T., et al., 1990, "Similarity Analysis of Tip Clearance Flow Structure," ASME paper 90-GT-153.

Crook, A., 1989, "Numerical Investigation of Endwall/Casing Treatment Flow Phenomena," M.S. Thesis, MIT.

Freeman, C., 1985, "Tip Clearance Effects in Axial Turbomachines," VKI Lecture Series 1985-05, April 15-19.

Kirtley, K.R., Beach, T.A., and Adamczyk, J.J., 1990, "Numerical Analysis of Secondary Flow in a Two-Stage Turbine," AIAA-90-2356.

Koch, C. C., 1981, "Stalling Pressure Rise Capability of Axial Flow Compressor Stages," ASME J. of Eng. for Power, Vol. 103, October 1981, pp. 645-656.

McDougall, N.M., 1990, "A Comparison Between the Design Point and Near-Stall Performance of an Axial Compressor," ASME Journal of Turbomachinery, Vol 112, No 1, pp 109-115.

McDougall, N.M., Cumpsty, N.A., and Hynes, T.P., 1990, "Stall Inception in Axial Compressors," ASME Journal of Turbomachinery, Vol 112, No 1, pp 116-125.

Miller, G.R. and Bailey, E.E., 1971, "Static-Pressure Contours in the Blade Passage at the Tip of Several High Mach Number Rotors," NASA TM X-2170.

Moore, F.K., 1984, "A Theory of rotating stall of multistage compressors," Part I-III, ASME Journal of Gas Turbine Power, Vol 106, pp 313-336.

Moore, F.K., Greitzer, E.M., also Greitzer, E.M. and Moore, F.K., 1986, "A Theory of Post-Stall Transients in Axial Compression Systems," Part I and II, ASME Journal of Engineering for Gas Turbines and Power, Vol 108, pp 231-239.

Moore, R. D., 1982, "Rotor Tip Clearance Effects on Overall and Blade-Element Performance of Axial-Flow Transonic Fan Stage," NASA TP 2049.

Nicholas, D.J. and Freeman, C., 1982, "Recent Advances in the Performance of High Bypass Ratio Fans," Presented at the 13th Congress of the International Council of Aeronautics (ICAS)/ AIAA Aircraft System and Technology Conference, held in Seattle, WA, August 22-27.

Schweitzer, J. K., Garberoglio, J. E., 1984, "Maximum Loading Capability of Axial Flow Compressors," J. Aircraft, Vol. 21, No. 8, August 1984, pp 593-600.

Smith, L.H., 1970, "Casing Boundary Layers in Multi-Stage compressors," Proceedings of the Symposium on Flow Research on Blading, Elseview Publishing Company.

Strazisar, A.J., Wood, J.R., Hathaway, M.D., and Suder, K.L., 1989, "Laser Anemometer Measurements in a Transonic Axial-Flow Fan Rotor," NASA TP 2879.

Wennerstrom, A.J., 1984, "Experimental Study of a High Through-Flow Transonic Axial Compressor Stage," ASME Journal of Engineering for Gas Turbines and Power, Vol 106, pp 552- 560.

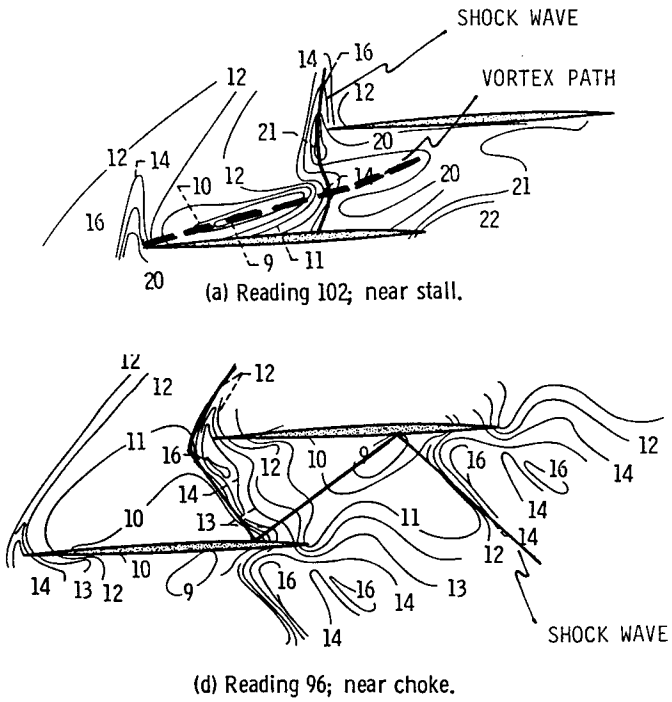

Figure 1. Pressure contours of a high-speed rotor, from Miller and Bailey (1971).

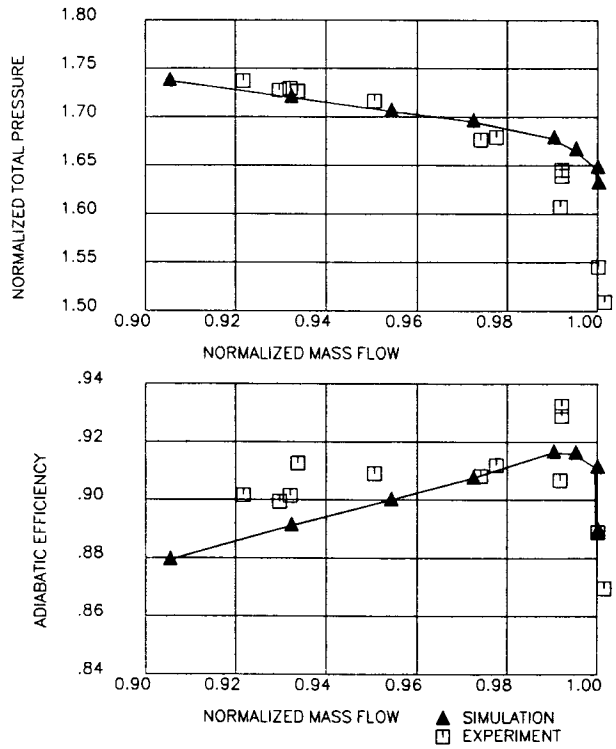

Figure 3. Comparison of predicted and measured pressure rise characteristic and adiabatic efficiency map of Rotor 67, Tip Clearance / Tip Chord = 0.25%.

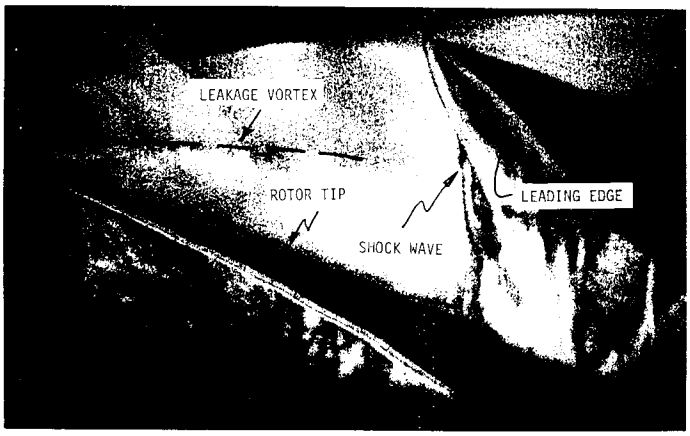

Figure 2. Photographic reproduction of a laser hologram of the tip flow field of a high-speed fan, from Nicholas and Freeman (1982).

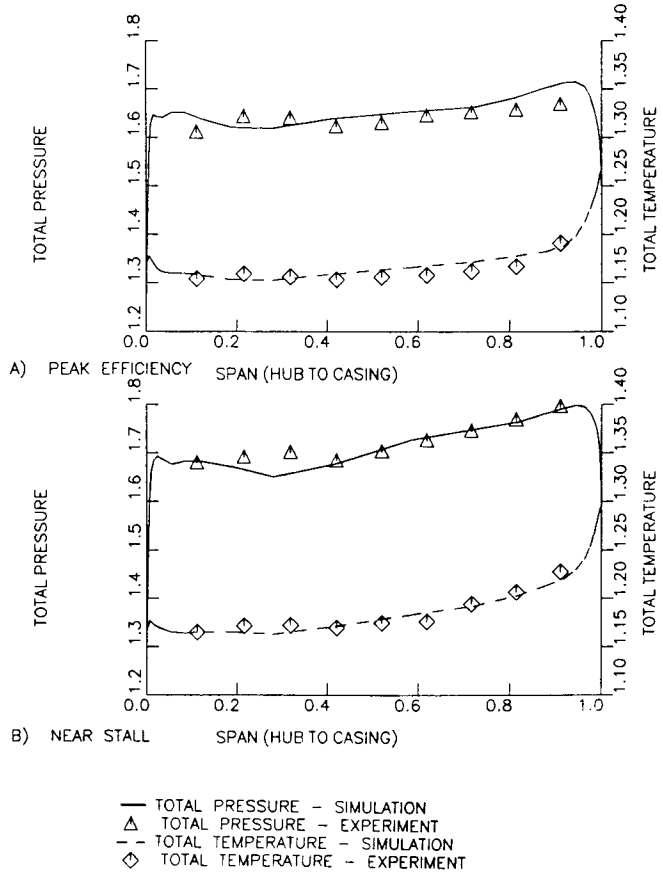

Figure 4. Comparison of predicted and measured axisymmetric-averaged and mass-averaged total pressure and total temperature profiles, Tip Clearance / Tip Chord = 0.25%.

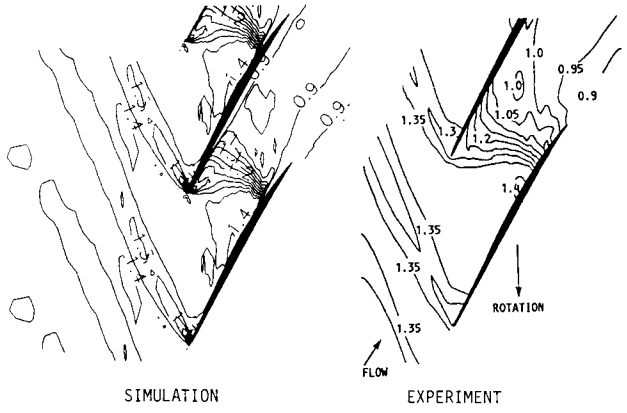

A) NINETY PERCENT SPAN FROM HUB

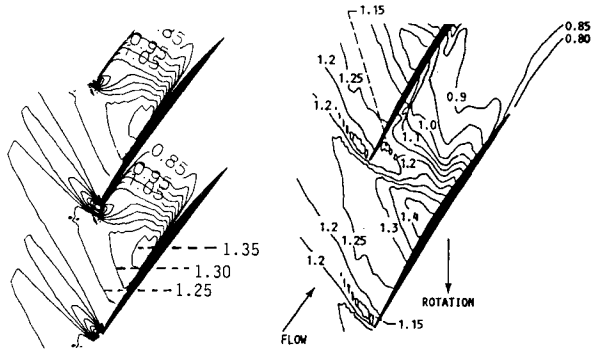

B) SEVENTY PERCENT SPAN FROM HUB

Figure 5. Comparison of predicted and measured intra-blade Mach number contours at ninety and seventy percent span at near peak efficiency, Tip Clearance / Tip Chord = 0.25%. (Contour Increments 0.05)

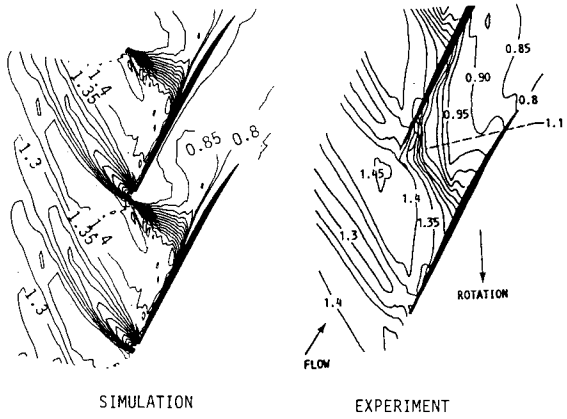

A) NINETY PERCENT SPAN FROM HUB

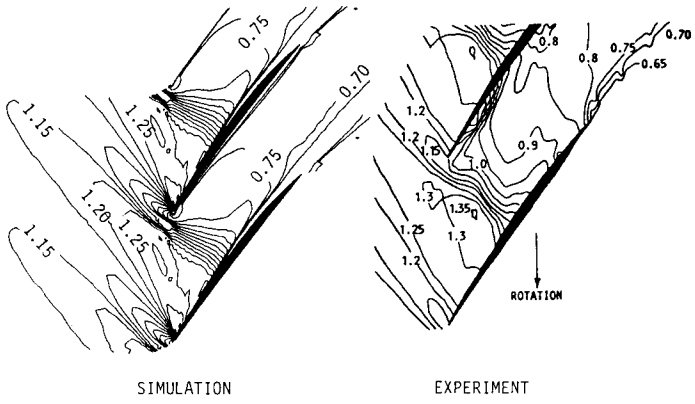

B) SEVENTY PERCENT SPAN FROM HUB

Figure 6. Comparison of predicted and measured intra-blade Mach number contours at ninety and seventy percent span at near stall, Tip Clearance / Tip Chord = 0.25%¿ (Contour Increments 0.05)

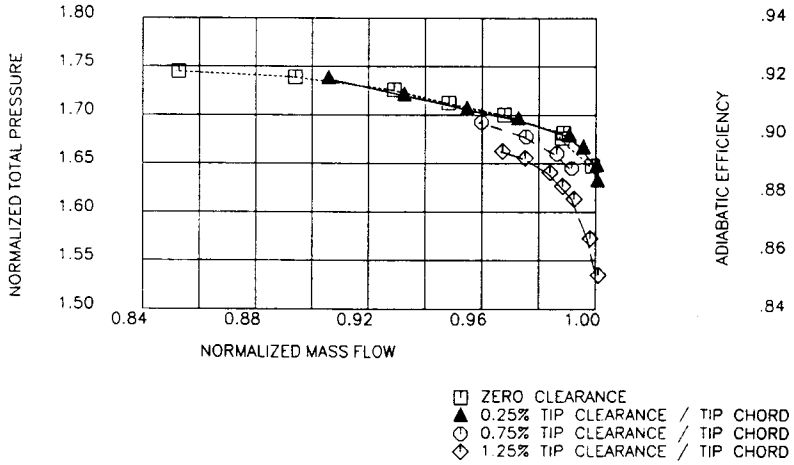

Figure 7. Comparison of predicted pressure rise characteristics and adiabatic efficiency maps of Rotor 67 for Tip Clearance / Tip Chord ratios of zero, 0.25, 0.75, and 1.25%.

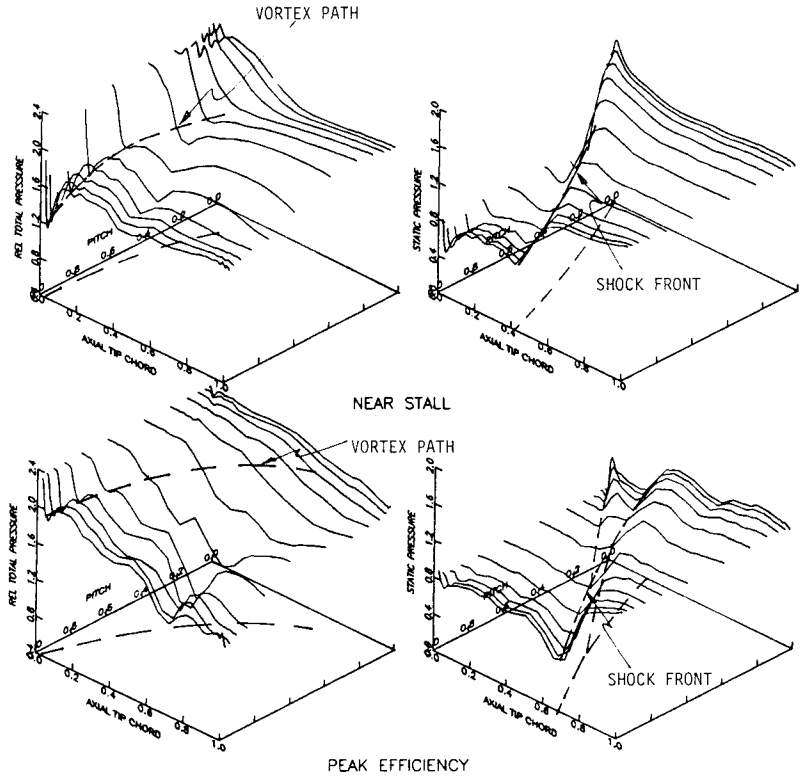

Figure 8. Relative total and static pressure in the clearance region, Tip Clearance / Tip Chord = 0.25%.

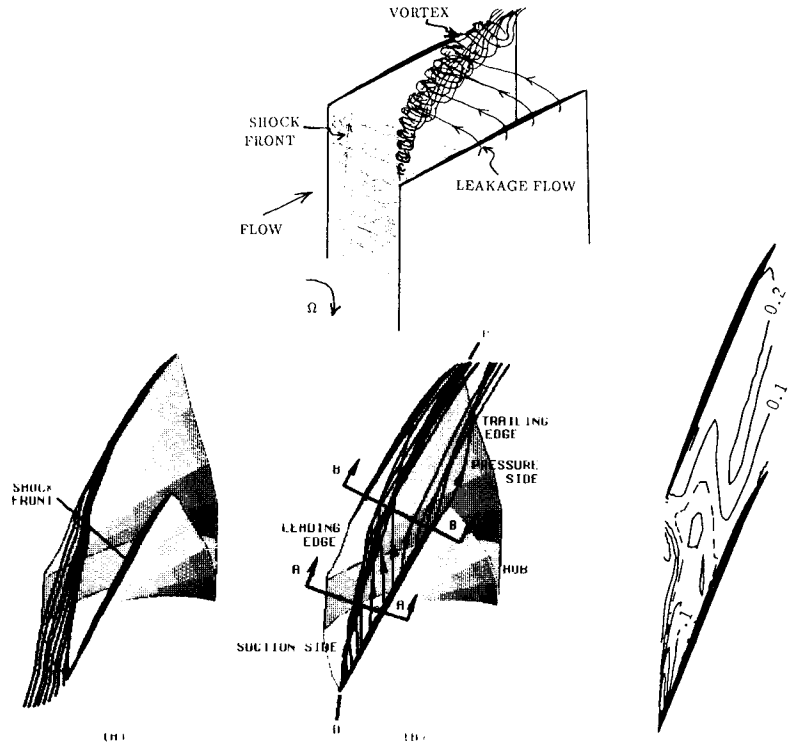

Figure 9. Illustration of the flow field in the tip clearance region at near stall by particle traces and contours of axial velocity at Tip Clearance / Tip Chord = 0.25%: (A) particles released upstream of the leading edge and restricted to blade-to-blade surface adjacent to the casing; (B) particles released near the suction surface; and (C) contours of axial velocity nondimensionalized by tip wheel speed (dashed contour denotes zero contour level).

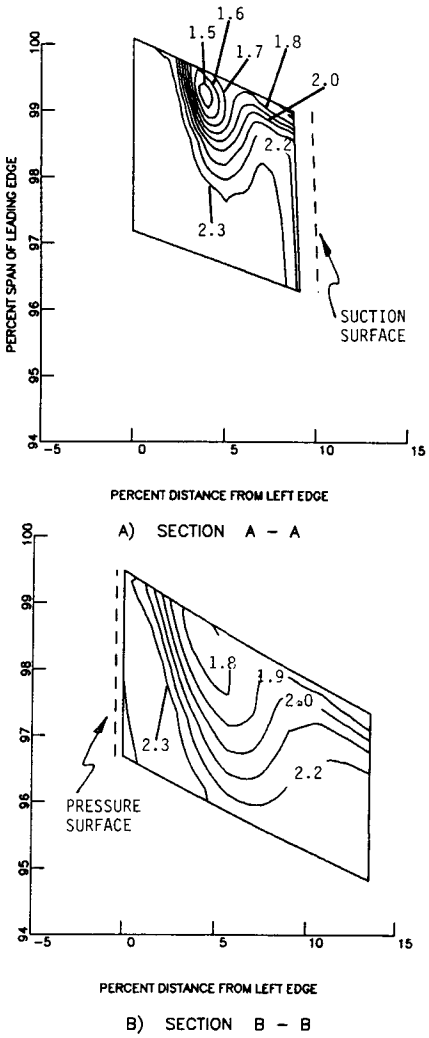

Figure 10. Sectional cuts of relative total pressure at near stall in the tip clearance region, Tip Clearance / Tip Chord = 0.25%.

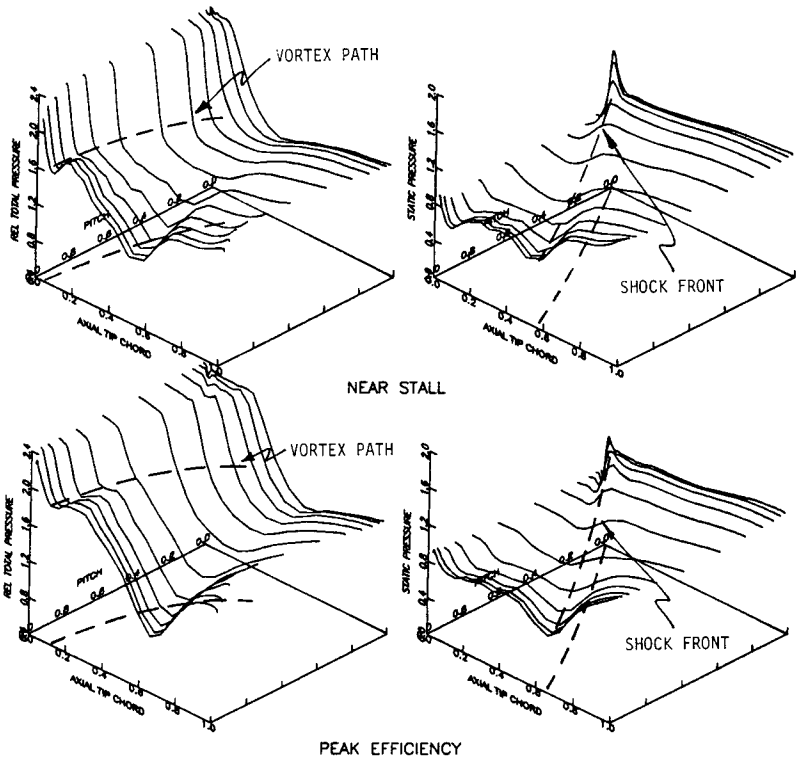

Figure 11. Relative total and static pressure in the clearance region, Tip Clearance / Tip Chord = 1.25%.

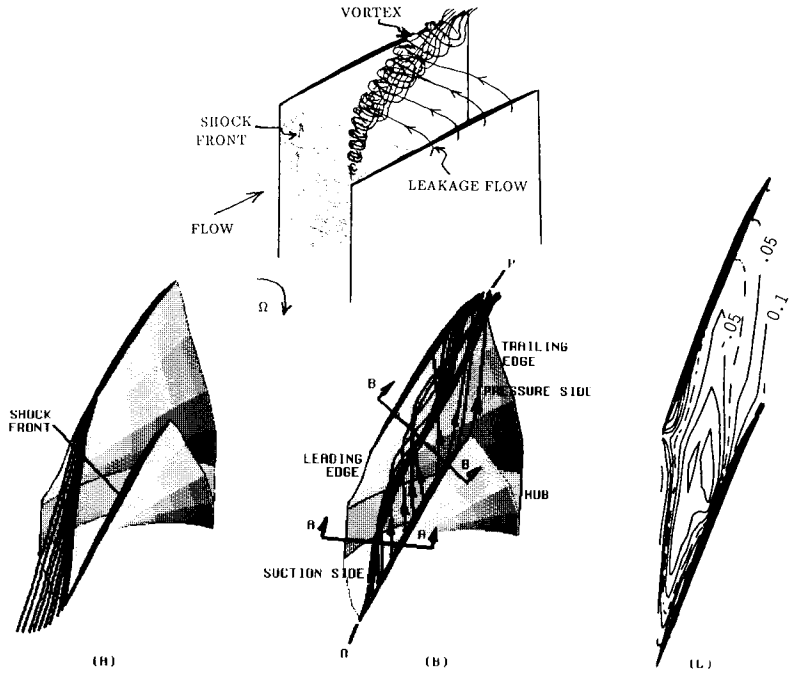

Figure 12. Illustration of the flow field in the tip clearance region at near stall by particle traces and contours of axial velocity at Tip Clearance / Tip Chord = 1.25%: (A) particles released upstream of the leading edge and restricted to blade-to-blade surface adjacent to the casing; (B) particles released near the suction surface; and (C) conturs of axial velocity nondimensionalized by tip wheel speed (dashed contour denotes zero contour level).

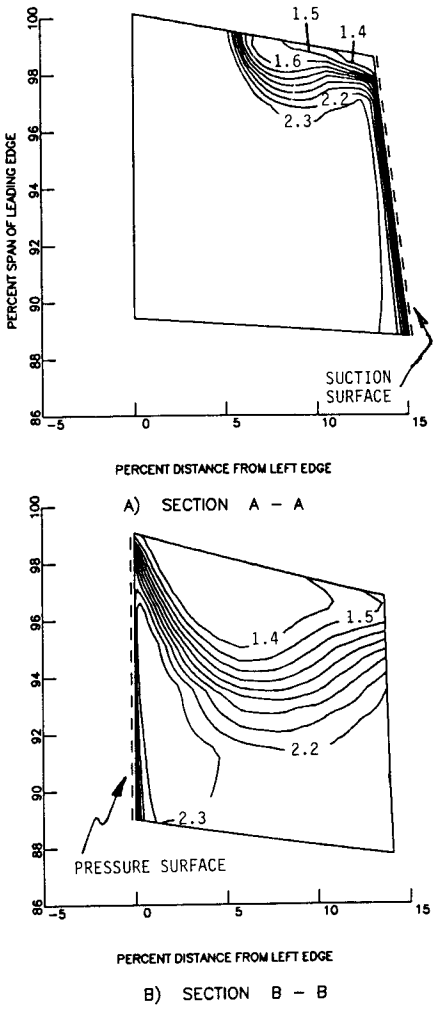

Figure 13. Sectional cuts of relative total pressure at near stall in the tip clearance region, Tip Clearance / Tip Chord = 1.25%.

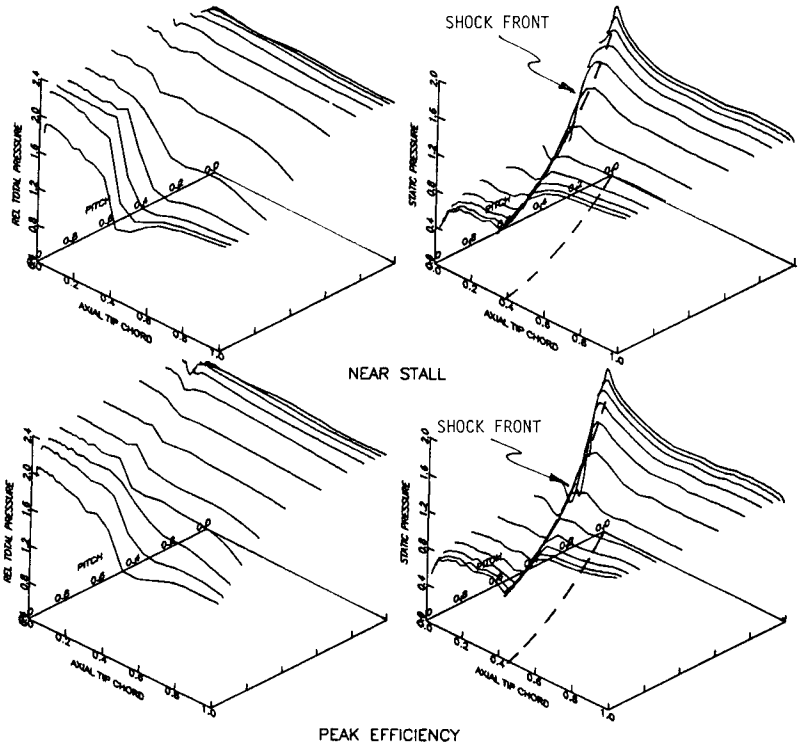

Figure 14. Relative total and static pressure in the clearance region, zero tip clearance.

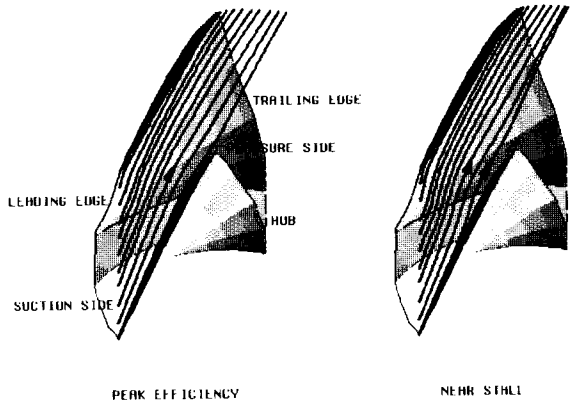

Figure 15. Particle traces injected upstream of the leading edge and restricted to blade-to-blade surface adjacent to the casing, zero clearance.

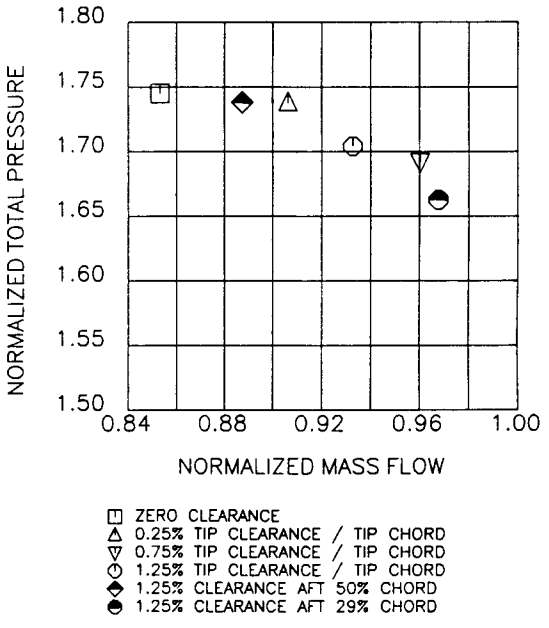

Figure 16. Predicted pressure ratio at near stall points for Tip Clearance / Tip Chord ratios of zero, 0.25, 0.75, 1.25%, and clearance of 1.25% aft of 29% and 50% chord.

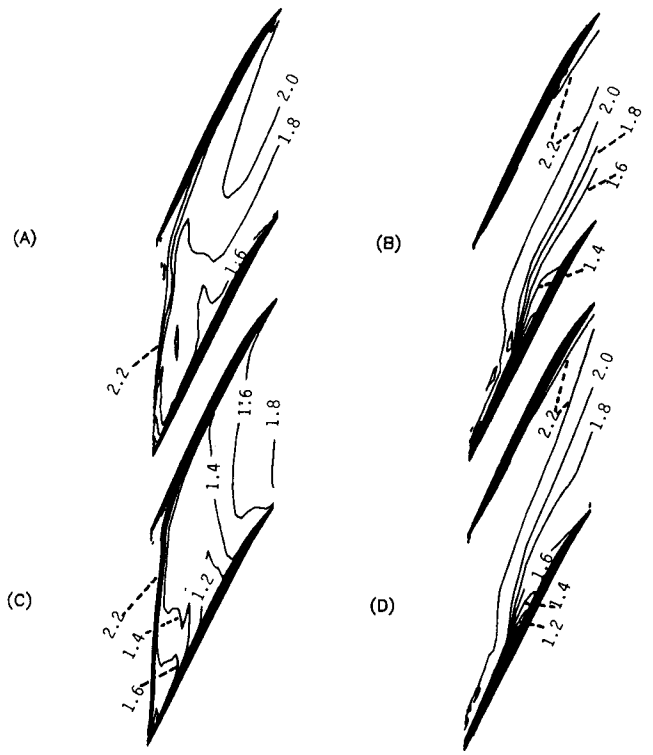

Figure 17. Blade-to-blade cut of relative total pressure at near stall flow at Tip Clearance / Tip Chord of: (A) 0.25%; (B) zero; (C) 1.25%; and (D) 1.25% aft of 50% chord.

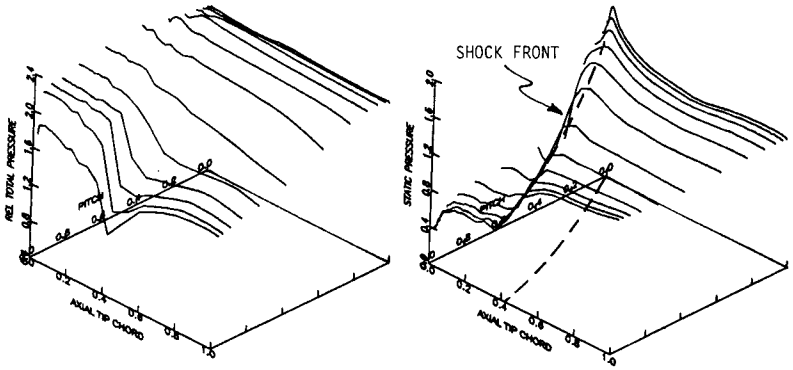

Figure 18. Relative total and static pressure in the clearance region at near stall, Tip Clearance / Tip Chord = 1.25% aft of 50% chord.